

Quasi-periodic oscillations in precursor flares via seismic aftershocks from resonant shattering

A. G. Suvorov^{1,2,*}, H. J. Kuan^{2,3}, and K. D. Kokkotas²

¹ Manly Astrophysics, 15/41-42 East Esplanade, Manly, NSW 2095, Australia

² Theoretical Astrophysics, IAAT, University of Tübingen, Tübingen, D-72076, Germany

³ Department of Physics, National Tsing Hua University, Hsinchu 300, Taiwan

Received ???; accepted ???

ABSTRACT

Context. GRB 211211A was accompanied by a kilonova, implying a merger origin for the event. A precursor flare, modulated by quasi-periodic oscillations at ≈ 22 Hz, was also seen ≈ 1 s prior to the main emission.

Aims. It is suggested here that the precursor resulted from the resonant shattering of one star's crust prior to coalescence. Seismic aftershocks and low-frequency torsional modes may emanate from the rupture site in this case, explaining the underlying oscillations. This interpretation is directly analogous to proposals for giant flares from soft gamma repeaters, where oscillations at similar frequencies have been observed, involving starquakes followed by crustal vibrations.

Methods. Torsional mode properties are computed for sequences of slowly-rotating, magnetised neutron stars in general relativity.

Results. The ≈ 22 Hz modulations in the precursor matches that of nodeless, $\ell = 2$ torsional modes for a wide variety of stellar parameters. Additionally, an analysis of the X-ray afterglow suggests that the merger remnant was a millisecond magnetar.

Key words. gamma-ray bursts: 211211A – stars: magnetars – stars: oscillations

1. Introduction

Gamma-ray bursts (GRBs) are observationally classified as being either long or short depending on their duration, T_{90} . Long GRBs are typically associated with supernovae, and in most cases are well-explained by a ‘collapsar’ model where a relativistic jet, formed at the heart of a core-collapse, comes to drill through the stellar envelope, eventually producing the observed gamma-rays (e.g., Bloom et al. 2002; Bromberg et al. 2012). Short GRBs instead arise from binary merger events involving at least one neutron star, and are often associated with kilonovae (e.g., Ciolfi 2018). GRB 211211A however challenges this simple dichotomy (see also Zhang et al. 2007, for the case of GRB 060614), as the event was not accompanied by a supernova but rather a kilonova, despite its long duration ($T_{90} \approx 34.3$ s; Gompertz et al. 2022; Rastinejad et al. 2022; Yang et al. 2022). This suggests that GRB 211211A originated from a merger.

GRB 211211A was preceded by a nonthermal, soft gamma-ray flash (‘precursor flare’) 1.08 ± 0.2 s prior to the main event (Xiao et al. 2022). This precursor flare, which is spectrally similar to those observed in short GRBs (Wang et al. 2020), may have launched prior to coalescence, at an orbital separation that depends on a sub-second jet-formation timescale, τ_{jet} (Zhang 2019). For the first time however, quasi-periodic oscillations (QPOs) at 22_{-2}^{+3} Hz were detected within the precursor flare at the $> 5\sigma$ level (Xiao et al. 2022). Although less significant, a second Fourier peak is also visible at 51 ± 2 Hz in the Fermi data (see extended data Figure 7 in Xiao et al. 2022).

Tidal resonances may be responsible for precursor flares from binary mergers (Tsang et al. 2012; Tsang 2013). The basic mechanism involves the excitation, via orbital resonances,

of stellar quasi-normal modes (QNMs) within one of the inspiralling constituents. If polar-parity QNM amplitudes reach a sufficiently high peak during the resonance window, the crust may strain enough that it fractures, releasing copious gamma-rays. Depending on the orbital frequency at the time of the precursor, different modes may be favoured, such as f - (Suvorov & Kokkotas 2020), i - (Neill et al. 2021), or g -modes (Kuan et al. 2021b).

Crustquakes are also popular models for giant flares in soft gamma repeaters (SGRs; Thompson & Duncan 1995). As first argued by Duncan (1998) (see also Blaes et al. 1989), global seismic oscillations are likely to accompany a fracture; torsional modes, which are restored by the weak Coulomb forces of crustal ions, are especially easy to excite in such a scenario. Torsional mode properties have been calculated by many authors at various levels of sophistication. General-relativistic (Schumaker & Thorne 1983), rotational (Lee & Strohmayer 1996; Vavoulidis et al. 2007), and especially magnetic (Messios et al. 2001; Sotani et al. 2007; Sotani & Kokkotas 2009; Colaiuda & Kokkotas 2011) effects, most relevant for magnetars, have been studied. The torsional eigenfunctions depend primarily on the shear modulus of the crust, μ (e.g., Tews 2017). Studies agree however that the nodeless, $\ell = 2$ modes (${}_2t_0$) for slowly rotating and modestly magnetised stars have frequencies in the range of $20 \lesssim {}_2t_0/\text{Hz} \lesssim 30$; $\ell = 4$ mode frequencies instead have $40 \lesssim {}_4t_0/\text{Hz} \lesssim 60$. If quakes are responsible for precursor flares, it is natural therefore that damped oscillations (i.e., QPOs) at these frequencies manifest within the spectrum.

Although the mechanism instigating the fracture differs, the excitation of torsional modes in GRB 211211A's precursor may be exactly analogous to that in SGRs, such as SGR 1900+14, where QPOs at frequencies of 28 ± 2 Hz, 53 ± 5 Hz, ~ 84 Hz, and 155 ± 6 Hz were detected in the tail of the 1998 giant flare (Hurley

* arthur.suvorov@manlyastrophysics.org

et al. 1999; Strohmayer & Watts 2005). We explore this scenario in this Letter. We complement our study with an analysis of the X-ray afterglow of the main event, which we find is well-fitted by a magnetar wind model (Rowlinson et al. 2013). This allows us to infer additional information about the event as a whole.

2. Precursor flare in GRB 211211A

The precursor in GRB 211211A was observed by Fermi/GBM, Swift/BAT, and Insight-HXMT/HE (Xiao et al. 2022). The waiting time of the precursor relative to the main event is found to be ~ 0.93 s for Fermi, ~ 0.88 s for Swift, and ~ 1.28 s from Insight data. Overall, therefore, we consider the waiting time to be 1.08 ± 0.2 s, which is not unusual for precursors in other merger-driven GRBs (e.g., GRBs 140209A and 181126413; Wang et al. 2020). This delay corresponds to an orbital frequency of $\Omega_{\text{orb}} \approx 400 \pm 40$ Hz, though could be higher if the jet-formation timescale $\tau_{\text{jet}} \gg 0$ (Zhang 2019). Such an Ω_{orb} is approximately twice that of the ${}_2g_2$ -mode eigenfrequency in a cold ($T \gtrsim 10^6$ K) neutron star; see Tab. 2 of Kuan et al. (2021b) and below.

2.1. Resonant shattering

A neutron star, spiralling around a companion, experiences a tidal field that perturbs its crustal matter. If the frequency of the perturbing force matches the frequency of a given QNM, said mode will become resonantly excited by efficiently depleting energy from the orbit. The amount of energy that can be transferred into the mode depends on its frequency and the degree of ‘tidal overlap’, which defines the coupling strength to the external tidal field (see, e.g., Alexander 1987; Kokkotas & Schafer 1995). If the overlap integral is large enough, the induced strain on the crust may exceed the elastic maximum, resulting in a failure (Tsang et al. 2012; Suvorov & Kokkotas 2020; Kuan et al. 2021b; Neill et al. 2021). With a binary-based kilonova model, Rastinejad et al. (2022) find best-fit masses (see their Fig. 7) for the progenitors as $M_1 = 1.43 \pm 0.05 M_{\odot}$ (primary) and $M_2 = 1.25 \pm 0.03 M_{\odot}$ (companion). We can use these as direct inputs for the resonant shattering aspect of the problem.

Fluid elements in a neutron star experience buoyancy whenever away from equilibrium if there are compositional or thermal gradients, or state changes (involving, e.g., superfluidity or superconductivity; Passamonti et al. 2016). These effects give rise to a rich spectrum of g -modes, with Brunt-Väisälä frequencies that depend on the Fermi energies of the various particle species and the internal temperature. These frequencies are calculated here by assuming the adiabatic indices of the perturbed star and (normal fluid) equilibrium have a fixed ratio, taken to be a ‘canonical’ value appropriate for a mature star; see Appendix A for details. Kuan et al. (2021b) show that ${}_2g_2$ -modes in this case can become resonant ~ 1 s prior to coalescence, exerting crust-breaking levels of strain if the stellar parameters lie in a particular range. For a wide library of equations of state (EOS) however, ${}_2g_2$ -modes for stars with $M \approx 1.4 M_{\odot}$ tend to be ‘tidally-neutral’, in the sense that the overlap integrals are comparatively small (see Appendix A of Kuan et al. 2022). It is therefore more difficult, at least within a g -mode resonance scenario (cf. Tsang et al. 2012; Neill et al. 2021), to accept a crust breaking for the primary, because the saturation amplitude is low.

If the companion fractures 1.08 ± 0.2 s prior to coalescence, constraints on the star’s spin frequency and magnetic field can be placed, as these shift the mode frequency. The aspects of the magnetic geometry (e.g., toroidal fields, multipoles) are im-

portant in this case. For simplicity, we adopt a dipole field, the specifics of which are given in Appendix A. Following Kuan et al. (2021b, 2022), we find that a ${}_2g_2$ -mode resonance can fracture a static star, at the right time (assuming $\tau_{\text{jet}} \approx 0$), for polar field strength $B_p = 7.78^{+0.41}_{-0.33} \times 10^{14}$ G, where the uncertainties account for the ~ 0.2 s window (Xiao et al. 2022); see Fig. A.1. The formation of a binary with such a component is unlikely (Popov & Prokhorov 2006), though cannot be ruled out *a priori*.

3. Seismic excitations

Xiao et al. (2022) identified, with $> 5\sigma$ significance, QPOs with frequency 22^{+3}_-2 Hz in the GRB 211211A precursor. Secondary Fourier peaks are also clearly visible at 51 ± 2 Hz in the Fermi spectrum (see extended data Figures 7 and 8 in Xiao et al. 2022). These QPO frequencies are similar to those found in the tails of SGR giant flares (Hurley et al. 1999; Israel et al. 2005).

There are a few possibilities for how low-frequency crustal modes may be excited coincidentally with a precursor.

- If indeed QNMs soak enough orbital energy, such that the resulting crustal strain exceeds the threshold of the lattice structure in the crust ~ 1 s prior to merger, aftershocks may excite torsional modes. Such a scenario is qualitatively identical to that put forth by Duncan (1998) for SGR flares.
- Some of the high-frequency mode’s energy may leak into lower frequency modes because of nonlinear couplings and parametric resonances (Dziembowski 1982; Pnigouras & Kokkotas 2015). Parametric excitation of torsional or shear modes, which are axial, likely requires however that the resonant mode responsible for the fracture is itself axial, since cross-parity modes couple only weakly. This is problematic because the radial shear of axial modes is negligible, and they therefore cannot break the crust. However, mixed poloidal-toroidal magnetic fields and rotation can couple the axial and polar sectors (Sotani & Kokkotas 2009; Colaiuda & Kokkotas 2011). If the flaring component in GRB 211211A is a magnetar (see Sec. 5), this scenario could be viable.
- Even if resonant shattering does not occur, shear or torsional modes may come into resonance with the tidal push prior to fracture. As torsional modes have long damping times (Schumaker & Thorne 1983), they could remain active until coalescence following a resonance at orbital frequency $\ll 100$ Hz. Although the relevant tidal overlap integrals are small, even weak vibrations in the crust could manifest within the precursor spectrum (Xiao et al. 2022).

The above scenarios can be explored with first-principles simulations. In the first case, the strain tensor, associated with the Lagrangian displacement of the resonant mode(s), can be used to deduce the fracture geometry given a chemical model of the crust (Suvorov & Kokkotas 2020; Kuan et al. 2021b). The resulting spatial profile can be projected into spheroidal harmonics, which serve as initial data for a torsional/shear perturbation problem. In this way, predictions for seismic excitations can be matched to exact fracture geometries, and resonance scenarios can be told apart. Observational avenues are also available. If QPOs are observed immediately (i.e., with zero time delay) following a fracture, aftershocks, which have some propagation time, could not be causally responsible. In such a case, the modes must be active prior to the precursor, pointing perhaps towards the third mechanism described above.

3.1. Quasi-periodic oscillations from aftershocks

A first-principles analysis, as described in the previous section, lies beyond the scope of this paper. We can, however, make some quantitative statements by computing the properties for free (i.e., without fracture seeding) torsional modes, assuming they are excited immediately after a tidal resonance. If the yielding is caused by a ${}_2g_2$ -mode (see Sec. 2.1), the cracking area¹ is confined near the equator, with colatitudes $0.25 \lesssim \theta/\pi \lesssim 0.75$ (see Fig. 3 in Kuan et al. 2021b). The angular distribution is similar to that of $\ell = m = 2$ harmonics. Modes with azimuth numbers $m \neq 2$ are largely decoupled from the perturbation due to mode orthogonality. Similarly, odd-order harmonics with $\ell = 3, 5, \dots$ are dormant because the ${}_2g_2$ -mode, seeding the fracture, is reflection symmetric about the equator. For GRB 211211A then, the modes of most interest are ${}_2t_0$ and ${}_4t_0$ (both with $m = 2$).

To calculate these, we closely follow the formalism described by Sotani et al. (2007); in particular, their equations (69) and (70) together with boundary conditions (71) and (72) completely describe the eigenproblem, including magnetic corrections, for torsional modes in the Cowling approximation. An input for these equations is the hydrostatic background, which is described by the Tolman-Oppenheimer-Volkoff equations for some EOS, with a separate model for the crust applied for low densities. We use the Akmal et al. (1998) (APR4) EOS for the core, together with a Douchin & Haensel (2001) fit for the crust. Colaiuda & Kokkotas (2011) found that modes associated with a $1.4M_\odot$ magnetar with this EOS exactly match the QPOs found in the giant flare tails of SGR 1806–20 and SGR 1900+14 (Israel et al. 2005). The final ingredient is the shear modulus, $\mu = (0.015 + 0.611\rho_{14} + 0.599\rho_{14}^2 - 0.349\rho_{14}^3 + 0.273\rho_{14}^4) \times 10^{30} \text{ erg cm}^{-3}$, with ρ_{14} being the mass density in units of $10^{14} \text{ g cm}^{-3}$; this fitting approximates the high charge-number (Z) profile calculated by Tews (2017); see Fig. 6 therein.

With the above specifications, we find ${}_2t_0^{(0)} = 24.22 \text{ Hz}$ and ${}_4t_0^{(0)} = 51.35 \text{ Hz}$ for a static, unmagnetised star with $M = 1.25M_\odot$. These already agree well with the Fourier peaks observed by Xiao et al. (2022), though shift slightly if rotational and magnetic corrections are applied. Combining these effects, we find, for $m = 2$, a hybrid fitting to the frequency shift, viz.

$$\frac{\ell t_n}{\ell t_n^{(0)}} = \sqrt{1 + \left(\frac{B_p}{\ell \tilde{B}_n}\right)^2} - \frac{2\nu(\ell^2 + \ell - 1)}{\ell t_n^{(0)} \ell(\ell + 1)} + O\left[\left(\frac{B_p}{\ell \tilde{B}_n}\right)^2, \left(\frac{\nu}{\ell t_n^{(0)}}\right)^2\right], \quad (1)$$

for fitting coefficients ${}_2\tilde{B}_n = 2.78 \times 10^{15} \text{ G}$ and ${}_4\tilde{B}_n = 2.65 \times 10^{15} \text{ G}$, where ℓt_n is the inertial-frame frequency when $\nu > 0$. Equation (1) is similar to Eq. (79) of Sotani et al. (2007) when $\nu = 0$, and Eq. (26) of Vavoulidis et al. (2007) when $B_p = 0$.

A variety of $\ell = 2$ and $\ell = 4$ torsional mode frequencies are collated in Table 1. Although the $\nu = B_p = 0$ mode frequencies match those of the QPOs in GRB 211211A, a ${}_2g_2$ -mode resonance is unable to explain the precursor in this case (see Appendix A). Additionally, a strong magnetic field ($B_p \gtrsim 10^{14} \text{ G}$) may be necessary to extract the requisite energy, that fuels the precursor, from the crust (see Sec. 5). Overall, we find that there are many possible combinations of modest spins, $0 \lesssim \nu/\text{Hz} \lesssim 3$, and polar field strengths, $7 \lesssim B_p/10^{14} \text{ G} \lesssim 8$, that can allow for the resonant shattering to occur at the correct time, and produce

¹ The crack geometry also depends on the failure criterion (e.g., von Mises or Tresca) and the (likely anisotropic) elastic maximum the crust can absorb, neither of which are certain for neutron star matter; see Baiko & Kozhberov (2017) for a discussion.

Table 1. Frequencies (3rd column) of nodeless torsional modes in the companion ($M_2 = 1.25M_\odot$), for a range of spins ν (1st column) and polar field strengths B_p (2nd column) via expression (1). The core EOS is APR4 (Akmal et al. 1998), while the Douchin & Haensel (2001) fit governs the crust, which occupies the outermost 0.973 km of the star; such a model is able to explain the QPOs observed in the giant flare tails of SGR 1806–20 and SGR 1900+14 (Colaiuda & Kokkotas 2011). Bold numbers match the QPOs in GRB 211211A’s precursor, and/or the spin and magnetic field strengths predicted if a ${}_2g_2$ -mode resonance breaks the crust $\sim 1.08 \pm 0.2 \text{ s}$ prior to coalescence; see Sec. 2.1.

ν (Hz)	B_p (10^{13} G)	Mode Freq. ($\ell = 2, \ell = 4$) (Hz)
0	0	24.22, 51.35
2	0	20.89, 47.55
4	0	17.55, 43.75
0	1	24.22, 51.35
0	10	24.24, 51.39
0	100	25.74, 54.88
0.5	80	24.37, 52.69
1	76	23.44, 51.52
2	72	21.69, 49.41

torsional modes with the observed frequencies. Three such combinations are shown in the last three rows of Tab. 1. A resonant shattering followed by seismic aftershocks is therefore a viable explanation for the events that led up to GRB 211211A.

4. Afterglow

The components in GRB 211211A are relatively light ($M_1 + M_2 \approx 2.68 \pm 0.08M_\odot$), suggesting the possibility of a neutron star merger remnant, rather than a black hole. From a three-component kilonova model, Rastinejad et al. (2022) estimate that $0.04 \pm 0.02M_\odot$ worth of r -process material was dynamically ejected via tidal torques and shock heating during merger. After coalescence, additional mass may be lost as material in the temporary accretion disc surrounding the merger site unbinds through viscous heating. Fujibayashi et al. (2018, 2020) show that, for a long-lived remnant, the post-merger ejecta mass can reach $\approx 30 - 40\%$ of the total disc mass, amounting to $\gtrsim 0.1M_\odot$. These considerations suggest a remnant mass of $M_{\text{rem}} \approx 2.5 \pm 0.1M_\odot$; a star at the lower end could stave off collapse for a number of spindown timescales if born with high angular momentum (e.g., Suvorov & Glampedakis 2022).

GRB 211211A displayed an X-ray afterglow, part of which could be supplied by a magnetar wind (Rowlinson et al. 2013; Ciolfi 2018). Following the method described in Suvorov & Kokkotas (2021), we fit the 0.3–10 keV Swift-XRT flux, F , with an orthogonal rotator braking by magnetic dipole torques in vacuum. We find best-fit values, assuming a radius $R_\star = 13 \text{ km}$, of

$$B_p^\star = 4.4_{-1.0}^{+0.9} \times 10^{14} \left(\frac{I_\star}{3 \times 10^{45} \text{ g cm}^2}\right) \left(\frac{\eta}{10^{-4}}\right)^{1/2} \left(\frac{13 \text{ km}}{R_\star}\right)^3 \text{ G} \quad (2)$$

and

$$\nu_\star = 1.26_{-0.15}^{+0.20} \left(\frac{3 \times 10^{45} \text{ g cm}^2}{I_\star}\right)^{1/2} \left(\frac{10^{-4}}{\eta}\right)^{1/2} \text{ kHz}, \quad (3)$$

for the remnant’s polar field strength and spin frequency, respectively, at a 95% confidence level. In estimating the above, we assume uncollimated emission and a conversion efficiency, from spindown power to X-ray power, of $\eta \approx 10^{-4}$, together with a photon index $\Gamma_\gamma = 2.08$ at source redshift $z = 0.0763$

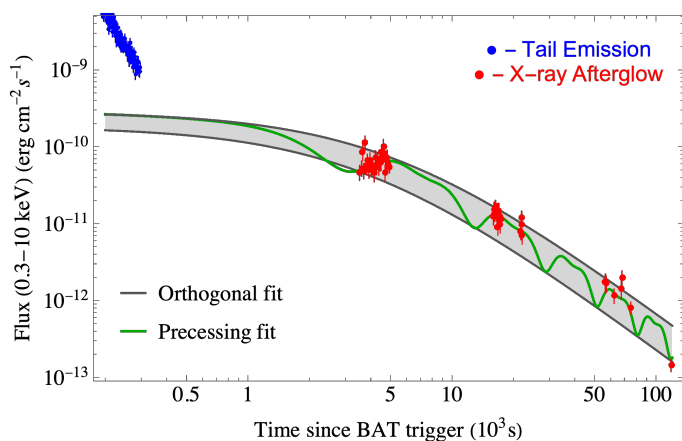


Fig. 1. Afterglow light-curve fittings for GRB 211211A. Blue data are attributable to the decaying tail of the prompt emission (Evans et al. 2014), while red data may be contributed by a newborn magnetar. The gray band shows the 95% confidence interval for an orthogonal-rotator fit, while the green curve shows a best-fit precessing model.

(Evans et al. 2014; Gompertz et al. 2022), translating into a source distance of $d \approx 350$ Mpc. This allows us to estimate the isotropic luminosity, viz. $L = 4\pi d^2 K(z)F$ for $K(z) \approx (1+z)^{\Gamma_\gamma-2}$ (Bloom et al. 2002). From numerical merger simulations with the APR4 EOS, Radice et al. (2018) find that the spin period for a newborn remnant is $P_\star \approx [-0.21 (M_{\text{rem}}/M_\odot - 2.5) + 0.67]$ ms, which agrees with expression (3). In addition to an orthogonal-rotator fit, we consider the possibility of a precessing remnant for completeness. Although the model specifics are complicated in this case (see Suvorov & Kokkotas 2021, for details), such a fit predicts similar parameters to the orthogonal case (within $\sim 30\%$), though with a quadrupolar ellipticity of $\epsilon \approx 1.3 \times 10^{-7}$ for the same efficiency and moment of inertia, I_\star .

Orthogonal (black) and precessing (green) fits to the afterglow light-curves of GRB 211211A are shown in Fig. 1. Overall, a magnetar wind model fits the data well, as they exhibit a power-law fall-off with slope -2 , as predicted by dipole braking.

5. Conclusions

If resonant shatterings are responsible for (at least some) precursor flares in merger-driven GRBs, seismic aftershocks may emanate from the rupture site shortly thereafter. We show that the ~ 22 Hz and ~ 51 Hz Fourier peaks observed in the precursor of GRB 211211A match those of $\ell = 2$ and $\ell = 4$ torsional modes for a variety of spin and magnetic field strength combinations (Tab. 1). These modes are expected based on the fracture geometry of ${}_2g_2$ -mode resonances, as quantified in Sec. 2.1. Even if a different mode is responsible for the resonant shattering (e.g., i -mode; Tsang et al. 2012), the same qualitative picture applies. Overall, the observation of QPOs in precursor flares may allow for detailed inferences regarding the flaring star’s properties.

The precursor showed no evidence for a thermal component (Xiao et al. 2022). As discussed by Tsang et al. (2012), this suggests that a magnetar participated in the merger. Essentially, energy is able to propagate as Alfvén waves along open field lines if B is large enough ($\gg 10^{13}$ G), and the spectrum will be predominantly nonthermal. Xiao et al. (2022) also find that the peak isotropic luminosity of the precursor is $7.4^{+0.8}_{-0.7} \times 10^{49}$ erg s $^{-1}$, which is rather high relative to other precursors (Wang et al. 2020). Tsang (2013) shows that the maximum luminosity, extractable from the crust of a star with radius R via the magnetic

field, is given by the surface integral

$$L_{\text{max}} = \int (\mathbf{v} \times \mathbf{B}) \times \mathbf{B} \cdot d\mathbf{A} \quad (4)$$

$$\sim 10^{49} (v/c) (B_{\text{surf}}/10^{14} \text{ G})^2 (R/10 \text{ km})^2 \text{ erg s}^{-1},$$

where \mathbf{v} is the velocity of the mode-related perturbation. The nonthermal character of the precursor, its relative timing (see Sec. 2.1), and the luminosity budget (4) all seem to demand magnetar-level fields for the flaring component in GRB 211211A. As such, not only may a magnetar have emerged from the crash site (as argued in Sec. 4), a magnetar may have been in the binary. Such considerations are relevant for population studies and evolutionary modelling of neutron stars (Popov & Prokhorov 2006).

Acknowledgements. The research leading to these results has received funding from the European Union’s Horizon 2020 Programme under the AHEAD2020 project (grant no. 871158). This work made use of data supplied by the UK Swift Science Data Centre at the University of Leicester. KK gratefully acknowledges financial support by DFG research Grant No. 413873357. HJK recognises support from Sandwich grant (JYP) No. 109-2927-I-007-503 by DAAD and MOST.

References

- Akmal, A., Pandharipande, V. R., & Ravenhall, D. G. 1998, *Phys. Rev. C*, 58, 1804
- Alexander, M. E. 1987, *MNRAS*, 227, 843
- Baiko, D. A. & Kozhberov, A. A. 2017, *MNRAS*, 470, 517
- Blaes, O., Blandford, R., Goldreich, P., & Madau, P. 1989, *ApJ*, 343, 839
- Bloom, J. S., Kulkarni, S. R., & Djorgovski, S. G. 2002, *AJ*, 123, 1111
- Bromberg, O., Nakar, E., Piran, T., & Sari, R. 2012, *ApJ*, 749, 110
- Cioffi, R. 2018, *International Journal of Modern Physics D*, 27, 1842004
- Colaiuda, A. & Kokkotas, K. D. 2011, *MNRAS*, 414, 3014
- Douchin, F. & Haensel, P. 2001, *A&A*, 380, 151
- Duncan, R. C. 1998, *ApJ*, 498, L45
- Dziembowski, W. 1982, *Acta Astron.*, 32, 147
- Evans, P. A., Osborne, J. P., Beardmore, A. P., et al. 2014, *ApJS*, 210, 8
- Fujibayashi, S., Kiuchi, K., Nishimura, N., Sekiguchi, Y., & Shibata, M. 2018, *ApJ*, 860, 64
- Fujibayashi, S., Wanajo, S., Kiuchi, K., et al. 2020, *ApJ*, 901, 122
- Gompertz, B. P., Rasio, M. E., Nicholl, M., et al. 2022, arXiv e-prints, arXiv:2205.05008
- Hurley, K., Cline, T., Mazets, E., et al. 1999, *Nature*, 397, 41
- Israel, G. L., Belloni, T., Stella, L., et al. 2005, *ApJ*, 628, L53
- Kokkotas, K. D. & Schafer, G. 1995, *MNRAS*, 275, 301
- Kuan, H.-J., Krüger, C. J., Suvorov, A. G., & Kokkotas, K. D. 2022, *MNRAS*, 513, 4045
- Kuan, H.-J., Suvorov, A. G., & Kokkotas, K. D. 2021a, *MNRAS*, 506, 2985
- Kuan, H.-J., Suvorov, A. G., & Kokkotas, K. D. 2021b, *MNRAS*, 508, 1732
- Lee, U. & Strohmayer, T. E. 1996, *A&A*, 311, 155
- Messios, N., Papadopoulos, D. B., & Stergioulas, N. 2001, *MNRAS*, 328, 1161
- Neill, D., Newton, W. G., & Tsang, D. 2021, *MNRAS*, 504, 1129
- Passamonti, A., Andersson, N., & Ho, W. C. G. 2016, *MNRAS*, 455, 1489
- Phigouras, P. & Kokkotas, K. D. 2015, *Phys. Rev. D*, 92, 084018
- Popov, S. B. & Prokhorov, M. E. 2006, *MNRAS*, 367, 732
- Radice, D., Perego, A., Bernuzzi, S., & Zhang, B. 2018, *MNRAS*, 481, 3670
- Rastinejad, J. C., Gompertz, B. P., Levan, A. J., et al. 2022, arXiv e-prints, arXiv:2204.10864
- Rowlinson, A., O’Brien, P. T., Metzger, B. D., Tanvir, N. R., & Levan, A. J. 2013, *MNRAS*, 430, 1061
- Schumaker, B. L. & Thorne, K. S. 1983, *MNRAS*, 203, 457
- Sotani, H. & Kokkotas, K. D. 2009, *MNRAS*, 395, 1163
- Sotani, H., Kokkotas, K. D., & Stergioulas, N. 2007, *MNRAS*, 375, 261
- Strohmayer, T. E. & Watts, A. L. 2005, *ApJ*, 632, L111
- Suvorov, A. G. & Glampedakis, K. 2022, *Phys. Rev. D*, 105, L061302
- Suvorov, A. G. & Kokkotas, K. D. 2020, *Phys. Rev. D*, 101, 083002
- Suvorov, A. G. & Kokkotas, K. D. 2021, *MNRAS*, 502, 2482
- Tews, I. 2017, *Phys. Rev. C*, 95, 015803
- Thompson, C. & Duncan, R. C. 1995, *MNRAS*, 275, 255
- Tsang, D. 2013, *ApJ*, 777, 103
- Tsang, D., Read, J. S., Hinderer, T., Piro, A. L., & Bondarescu, R. 2012, *Phys. Rev. Lett.*, 108, 011102
- Vavoulidis, M., Stavridis, A., Kokkotas, K. D., & Beyer, H. 2007, *MNRAS*, 377, 1553
- Wang, J.-S., Peng, Z.-K., Zou, J.-H., Zhang, B.-B., & Zhang, B. 2020, *ApJ*, 902, L42
- Xiao, S., Zhang, Y.-Q., Zhu, Z.-P., et al. 2022, arXiv e-prints, arXiv:2205.02186
- Yang, J., Zhang, B. B., Ai, S. K., et al. 2022, arXiv e-prints, arXiv:2204.12771
- Zhang, B. 2019, *Frontiers of Physics*, 14, 64402
- Zhang, B., Zhang, B.-B., Liang, E.-W., et al. 2007, *ApJ*, 655, L25

Appendix A: Magnetic field and spin inferences from precursor timing

As discussed in Secs. 2.1 and 3, mode frequencies are shifted by Coriolis and Lorentz forces. Quantifying these effects requires a particular model; the one used in the main text is detailed here. The relative shifts also depend on the mode eigenfunction. For torsional modes, the shifts are given by expression (1) in the main text, while for g -modes the patterns are different. In either case, specifying the nuclear EOS – assumed APR4 in this work because Colaiuda & Kokkotas (2011) found that torsional modes in a $M \approx 1.4M_\odot$ star with this EOS match the QPO frequencies in the giant flare tails of SGR 1806–20 and SGR 1900+14 (Israel et al. 2005) – uniquely determines the former if the star is uniformly rotating. Relative to a static-star mode, we find that the leading-order, rotational corrections to $m = 2$ modes, ${}_\ell\omega_n$, in geometrised units with $G = c = 1$, read [see Eqs. (17) and (18) in Kuan et al. (2021b)]

$${}_\ell\delta\omega_n^{\text{Cor}} = -4\pi\nu(1 - C_{n\ell}), \quad (\text{A.1})$$

with

$$C_{n\ell} = \frac{1}{MR^2} \int dr(p + \rho)e^{\Phi+\lambda}r^{2\ell-2}(\xi_r\bar{\xi}_h + \bar{\xi}_r\xi_h + \xi_h\bar{\xi}_h), \quad (\text{A.2})$$

for mode eigenfunction ξ , decomposed into radial (ξ^r) and poloidal (ξ^h) harmonics, stellar pressure p and density ρ , related to the metric functions Φ and λ , defining the (logarithms of the) g_{tt} and g_{rr} components respectively, via the Tolman-Oppenheimer-Volkoff relations. In the Newtonian limit, the above agrees with the classic Unno formula.

Although the presence of multipoles or a toroidal field can lead to sizeable adjustments in the Lorentz-related frequency shift (see, e.g., Colaiuda & Kokkotas 2011; Suvorov & Kokkotas 2020; Kuan et al. 2021a), a purely dipole configuration for the magnetic field is taken here for simplicity. Following Kuan et al. (2021a), it can be shown that relations of the Faraday tensor imply that a general, stationary and axisymmetric magnetic field has contravariant components

$$B^\mu = \frac{B_p}{2} \left(0, \frac{e^{-\lambda}}{r^2 \sin \theta} \frac{\partial \psi}{\partial \theta}, -\frac{e^{-\lambda}}{r^2 \sin \theta} \frac{\partial \psi}{\partial r}, -\frac{\zeta(\psi)\psi e^{-\Phi}}{r^2 \sin^2 \theta} \right), \quad (\text{A.3})$$

in Schwarzschild-like coordinates, where ζ is a toroidal function, which we set to zero. For a dipole field, the streamfunction ψ can be expressed as

$$\psi(r, \theta) = f(r) \sin^2 \theta, \quad (\text{A.4})$$

for some radial function f . We pick² $f(r) = a_1 r^2 + a_2 r^4 + a_3 r^6$, where the a_i are constrained by assuming that (I) the \mathbf{B} field smoothly extends to a force-free dipole outside of the star (where the geometry is Schwarzschild), and (II) that there are no surface-currents. Enforcing these conditions leads to

$$a_1 = -\frac{3R^3}{8M^3} \left[\log \left(1 - \frac{2M}{R} \right) + \frac{M(24M^3 - 9M^2R - 6MR^2 + 2R^3)}{R^2(R - 2M)^2} \right], \quad (\text{A.5a})$$

$$a_2 = \frac{3(12M - 7R)}{4R(R - 2M)^2}, \quad (\text{A.5b})$$

² To avoid confusion, we note that the function $f(r)$ is denoted by $a_1(r)$ in Sotani et al. (2007), which affects the spectrum of torsional modes via the associated terms in Eqs. (69) and (70) therein.

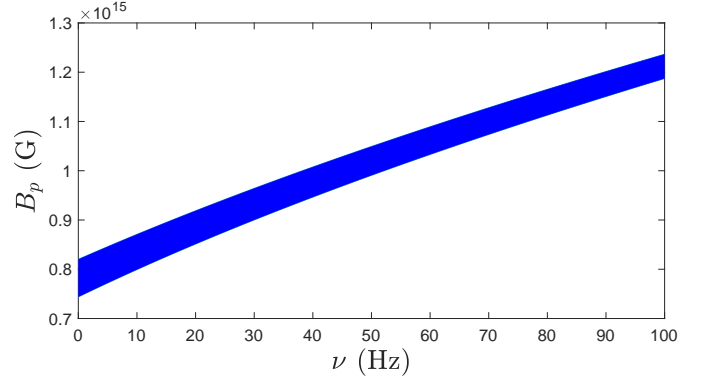


Fig. A.1. Polar magnetic field strengths B_p , as a function of spin ν , such that the resonance of a ${}_2g_2$ -mode is able to instigate a crust yielding at the observed preceding time, $T_{\text{wait}} = 1.08 \pm 0.2$ s, assuming a negligible jet-formation time, $\tau_{\text{jet}} = 0$, in GRB 211211A. The shaded region reflects the uncertainty in the waiting time.

and

$$a_3 = \frac{3(5R - 8M)}{8R^3(R - 2M)^2}. \quad (\text{A.5c})$$

Given this field, the Lorentz force F_μ^{Lor} can be defined, which leads to a frequency shift in the unmagnetised value, viz.

$${}_\ell\delta\omega_n^{\text{Lor}} = \frac{1}{2} \frac{\int_{\text{vol}} F_\mu^{\text{Lor}} \xi^\mu \sqrt{-gd^3x}}{\ell\omega_n \int_{\text{vol}} (\rho + p) e^{-2\Phi} \xi^\mu \bar{\xi}_\mu \sqrt{-gd^3x}}. \quad (\text{A.6})$$

The matching of the ${}_2g_2$ -mode to the precursor time implies a relationship between B_p and ν , for a given mass and stratification, i.e., we solve $2\Omega_{\text{orb}} = {}_2\omega_2 + {}_2\delta\omega_2^{\text{Cor}} + {}_2\delta\omega_2^{\text{Lor}} = 2\pi {}_2g_2$ in the inertial frame, implicitly assuming spin-orbit alignment (Alexander 1987; Kokkotas & Schafer 1995). We assume $M = 1.25M_\odot$, as identified by Rastinejad et al. (2022) for the companion in GRB 211211A (see Sec. 2.1). The stratification is encoded by a phenomenological parameter that incorporates the particle Fermi energies and internal temperature, called δ in Kuan et al. (2021b, 2022). In general, the equilibrium adiabatic index reads

$$\gamma(r) = \frac{\rho + p}{p} \frac{\partial p}{\partial \rho}, \quad (\text{A.7})$$

which we relate to the index of the perturbed star, Γ , through

$$\Gamma(r) = \gamma(1 + \delta). \quad (\text{A.8})$$

The frequencies of thermal g -modes are however much more sensitive to the surface temperature (see Sec. 2.1 of Kuan et al. 2022, for quantifications). We assume δ is a constant that is set by the value in the crust; a ‘canonical’ value, appropriate for a mature neutron star, is adopted, viz. $\delta = 0.005$ (justified in Kuan et al. 2022). This eventually yields values for ${}_2\omega_2$, and the ${}_2g_2$ -mode frequency can now be written as a function of B_p and ν .

Figure A.1 shows simultaneous estimates on B_p and ν , based on the above procedure, with the shaded area representing the uncertainty (i.e., $T_{\text{wait}} = 1.08 \pm 0.2$ s). For all spin frequencies, we find that magnetar-level fields of $B_p \gtrsim 7 \times 10^{14}$ G are required. Fields of this strength are consistent with the precursor energetics and nonthermality, discussed in Sec. 5. Though not shown, non-zero values for τ_{jet} imply even higher field strengths.

We emphasise that, although Fig. A.1 pertains to ${}_2g_2$ -modes, similar graphs may be drawn for other resonant shattering scenarios (involving, for example, i - or s -modes; Tsang et al. 2012; Neill et al. 2021). g -modes, with the simple one-parameter characterisation (A.8), are only considered here for concreteness.